Automotive Experiences
Vol. 9 No. 2 (2026) pp. 512-529
p-ISSN: 2615-6202 e-ISSN: 2615-6636

Research Paper

Assessment of Ride Comfort Enhancement in a Full Vehicle Active Suspension System Using Sliding Mode and Fuzzy Logic Control

Asma Al-Tamimi[1], Ahmad Al-Jarrah[1], Mohammad Salah[2], Suleiman Banihani[1], Samer Mutawe[1]

[1]Mechatronics Engineering Department, Faculty of Engineering, The Hashemite University, Jordan
[2]College of Engineering and Technology, American University of the Middle East, Kuwait

Mohammad.Salah@aum.edu.kw

https://doi.org/10.31603/ae.16114

Published by Automotive Laboratory of Universitas Muhammadiyah Magelang

Article Info
Submitted: 02/02/2026
Revised: 17/07/2026
Accepted: 21/07/2026
Online first: 16/08/2026

Abstract

Vehicle suspension systems play a crucial role in ensuring ride comfort, stability, and safety under varying road conditions. While conventional passive suspensions offer limited adaptability, active suspension systems dynamically regulate actuator forces to counteract road-induced disturbances and improve overall performance. This paper introduces and comparatively evaluates two control strategies, sliding mode control and fuzzy logic control, for a full-vehicle active suspension system, aiming to achieve vibration suppression and ride comfort enhancement. Comprehensive simulations were performed in MATLAB/Simulink environment under three severe deterministic road-disturbance profiles with amplitudes ranging from −15 cm to +20 cm. The results demonstrate that both controllers effectively suppress full-vehicle vibrations under challenging road disturbances. Using SMC as the comparative reference, FLC achieved up to a 69.5% reduction in maximum vertical displacement and a 97.5% reduction in peak vertical acceleration, while maintaining a steady-state tracking error below 0.89 cm and comparable control effort. The study's key contribution lies in demonstrating the superior vibration-suppression and ride-comfort performance of FLC relative to the implemented SMC in a full-vehicle active suspension system.. The large reduction in peak acceleration is mainly associated with the smoother control action of FLC compared with the switching-induced acceleration fluctuations of the implemented SMC. The main contribution of this study is a systematic comparative assessment of decentralized SMC and FLC under identical coupled full-vehicle suspension dynamics and severe asymmetric road disturbance.

Keywords: Full active suspension; Ride comfort; Vibration suppression; Sliding mode control; Fuzzy logic control

1. Introduction

The quest for improved ride comfort, vehicle stability and safety has driven significant advancements in automotive suspension systems. Among these, active suspension systems have emerged as a promising solution due to their ability to adapt to varying road conditions and driving dynamics by generating control forces using an external actuator. Unlike passive and semi-active suspension systems, which rely on fixed parameters or limited energy dissipation, active suspension systems offer superior performance by actively controlling the suspension dynamics. However, the inherent nonlinearities, uncertainties and external disturbances associated with these systems present substantial challenges in achieving precise and robust control. Addressing these challenges requires advanced control strategies capable of handling complex system dynamics while ensuring stability and performance [1], [2]. Salah in [3] designed and constructed a laboratory test rig for this purpose. The rig enables the study and

Nomenclature

α_1, α_2	control gains	m_{ui}	unsprung wheel mass, kg, where *i* represents the wheel order
β_1, β_2	control gains	m_{uf}	front unsprung wheel mass, kg
γ_1, γ_2	control gains	m_{ur}	rear unsprung wheel mass, kg
$\ddot{\theta}_s$	sprung vehicle body pitching acceleration, rad/s^2	s	linear sliding surface and switching function
$\dot{\theta}_s$	sprung vehicle body pitching rate, rad/s	u_i	active suspension wheel actuator force, N, where *i* represents the wheel order
θ_s	sprung vehicle body pitching angle, rad	z_{ri}	disturbance on each wheel, m, where *i* represents the wheel order
θ_{sd}	desired sprung vehicle body pitching angle, rad	z_{sdi}	desired sprung vehicle body corner vertical displacement, m, where *i* represents the wheel order
λ	positive constant that represents the slope of the sliding surface	$\dot{z}_{si}$	sprung vehicle body corner vertical velocity, m/s, where *i* represents the wheel order
$\ddot{\varphi}_s$	sprung vehicle body rolling acceleration, rad/s^2	z_{si}	sprung vehicle body corner vertical displacement, m, where *i* represents the wheel order
$\dot{\varphi}_s$	sprung vehicle body rolling rate, rad/s	$\ddot{z}_{ui}$	unsprung wheel mass vertical acceleration, m/s^2, where *i* represents the wheel order
φ_s	sprung vehicle body rolling angle, rad	$\dot{z}_{ui}$	unsprung wheel mass vertical velocity, m/s, where *i* represents the wheel order
φ_{sd}	desired sprung vehicle body rolling angle, rad	z_{ui}	unsprung wheel mass vertical displacement, m, where *i* represents the wheel order
a	part of vehicle side dimension, m	I_p	vehicle pitch inertia, kg·m^2
b	part of vehicle side dimension, m	I_r	vehicle roll inertia, kg·m^2
b_f	front vehicle damping coefficient, N/m	RP_d	reduction percentage for the sprung vehicle body mass vertical displacement, %
b_r	rear vehicle damping coefficient, N/m	RP_a	reduction percentage for the sprung vehicle body mass vertical acceleration, %
$\dot{e}_i$	error signal first-time derivative at each sprung vehicle body corner where *i* represents the wheel order	T_f	front vehicle width, m
e_i	error signal at each sprung vehicle body corner where *i* represents the wheel order	T_r	rear vehicle width, m
k_f	front vehicle body spring stiffness, N/m	$\ddot{Z}_s$	sprung vehicle body vertical acceleration, m/s^2
k_r	rear vehicle body spring stiffness, N/m	$\dot{Z}_s$	sprung vehicle body vertical velocity, m/s
k_{tf}	front tire stiffness, N/m	Z_s	sprung vehicle body vertical displacement, m
k_{tr}	rear tire stiffness, N/m	Z_{sd}	desired sprung vehicle body vertical displacement, m
m_s	sprung vehicle body mass, kg		

analysis of road terrain effects on automotive suspension systems and provides a platform for testing various control algorithms to evaluate their impact on suspension performance.

Nonlinear control techniques have gained prominence in the field of active suspension systems due to their ability to manage the system's nonlinear behavior effectively. Among these techniques, Sliding Mode Control (SMC) has been widely studied and applied due to its inherent robustness against parameter variations and external disturbances [4], [5], [6], [7], [8]. SMC operates by driving the system states to a predefined sliding surface and maintaining them there, ensuring insensitivity to matched uncertainties and disturbances. This characteristic makes SMC particularly suitable for active suspension systems, which are subject to varying road conditions, load changes and actuator limitations. However, traditional SMC is often associated with chattering, a high-frequency oscillation phenomenon, that can degrade system performance and cause actuator wear. Recent advancements in SMC, such as higher-order sliding modes, adaptive SMC and intelligent SMC, have sought to mitigate these issues while retaining the method's robustness [9], [10], [11].

The development of active suspension systems has been a subject of extensive research, traditionally relying on conventional and linear control techniques. Early studies focused on the application of Linear Quadratic Regulator (LQR) and H_∞ control to mitigate road disturbances [12], [13], [14]. As research progressed, algorithms such as Model Predictive Control (MPC) and backstepping were utilized to handle operational constraints and improve the trade-off between ride quality and suspension travel [15], [16], [17]. Wu *et al*. in [15] developed an attitude tracking control system for an All-Terrain Vehicle (ATV) using Tandem Active–Passive Suspension (TAPS). They compared LQR and MPC algorithms in simulations and real tests, finding that MPC offered better tracking and disturbance rejection. Their results highlight the effectiveness of TAPS with MPC for improving ride comfort and stability on rough terrain. Al-Jarrah *et al*. in [14] used an H2 optimal control strategy for full vehicle active suspension systems, where the controller was designed to reduce the effects of road disturbances and ensure a stable and comfortable ride for vehicle occupants. Also, Salah *et al*. in [18] proposed a robust nonlinear control scheme for active suspension systems to overcome the road disturbances and ensure a comfortable ride. The controller targeted a hydraulic or pneumatic actuator to guarantee zero vertical acceleration and velocity at the passenger or cargo cabinet. Lin *et al*. [16] used a backstepping control design scheme to improve the tradeoff between ride quality and suspension travel. Gohrle *et al*. in [17] utilized two MPC approaches for active suspension. The system was linearized using a local Jacobian linearization approach that is effective only in the vicinity of the system equilibrium point.

While these methods provided a solid foundation for suspension control, their real-world performance is often limited by their strict dependence on precise mathematical models, making it difficult to handle the system's highly nonlinear dynamics and uncertainties [19], [20].

To address these nonlinearities and bypass rigid modeling requirements, researchers have increasingly turned to intelligent and soft-computing methodologies. Multi-objective controllers [21], Deep Reinforcement Learning (DRL) strategies [22], and state least squares-based neural networks [23] have been successfully implemented to manage unknown road disturbances. Specifically, Fuzzy Logic (FL) algorithms have proven highly effective in isolating vibrations by relying on rule-based decision-making rather than exact system equations, adapting seamlessly to time-varying parameters in active and semi-active setups [24], [25], [26], [27], [28], [29], [30].

Ming *et al*. in [22] used a DRL strategy, and the control of the semi-active suspension using the Deep Deterministic Policy Gradient (DDPG) algorithm was introduced. Chen *et al*. in [21] utilized a multi-objective controller with a generalized norm to obtain the time-domain hard constraints. Al-Tamimi *et al*. in [23] used a state least squares-based neural network controller to control full vehicle active suspension systems with unknown road disturbances affecting the entire vehicle system. Ro *et al*. in [24] proposed a FL algorithm for active ride comfort of a quarter-car model. An active element in the model was also utilized in [25] and [26] with FLCs.

Parallel to these intelligent methods, robust nonlinear techniques, most notably SMC have been widely studied due to their inherent insensitivity to matched uncertainties and external disturbances [4], [5], [6], [7], [8], [31], [32]. SMC guarantees stability by driving the system states to a predefined sliding surface. However, traditional SMC is notoriously susceptible to chattering high-frequency control oscillations that can rapidly degrade ride comfort and cause premature actuator wear. To mitigate this drawback, recent advancements have heavily focused on adaptive SMC [31], [32], finite-time convergence schemes [33], and higher-order sliding modes such as super-twisting algorithms [9], [10], [11], [34], [35], [36], [37]. Furthermore, hybrid approaches have successfully integrated intelligent techniques, such as FL, with SMC to balance adaptability with mathematical robustness [38], [39]. Gang in [33] utilized fault-tolerant and finite-time convergence schemes in the design of a SMC for active vehicle suspension systems. Sam *et al*. in [38] proposed a PI-SMC approach for active suspension systems, which combined the robustness of SMC with the adaptability of FL. Also, Choi and Han in [39] developed a SMC strategy for electrorheological seat suspensions, incorporating a human-body model to improve ride comfort.

Despite extensive advances in active suspension control, a more specific gap remains in the direct comparative evaluation of fundamentally different nonlinear control strategies under identical, fully coupled four-wheel suspension dynamics. In the present study, the implemented SMC and FLC generate their control actions from local error-related signals without explicitly using the complete 7-DOF vehicle model in the online control computation. Nevertheless, they employ fundamentally different control mechanisms. The SMC uses a switching-based nonlinear control action derived from the tracking error and its derivative, providing strong disturbance-rejection capability but potentially introducing chattering and associated acceleration fluctuations. In contrast, the FLC employs a continuous rule-based inference mechanism that accommodates nonlinear behavior without requiring an explicit mathematical vehicle model in its control formulation. Accordingly, this study provides a consistent comparison of switching-based SMC and rule-based FLC under the same coupled full-vehicle suspension dynamics.

Consequently, the specific research gap addressed in this study is the limited direct comparative assessment of decentralized SMC and FLC under identical coupled four-wheel suspension dynamics, particularly under severe asymmetric disturbances that simultaneously excite heave, pitch, and roll motions.

The specific contributions of this work are: (1) Decentralized control of coupled full-vehicle dynamics: implementation and comparative evaluation of decentralized Single-Input Single-Output (SISO)-based SMC and FLC on a fully coupled four-wheel vehicle model, where four local controllers collectively suppress heave, pitch, and roll responses without requiring a centralized Multiple-Input Multiple-Output (MIMO) control architecture. (2) stress testing under severe asymmetric disturbances by evaluating both controllers under challenging road profiles with amplitudes reaching +20 cm and −15 cm to assess their disturbance-rejection performance under strongly coupled vehicle dynamics. (3) Chattering and acceleration-suppression analysis by quantitative comparison of the switching behavior of the implemented SMC with the smoother FLC action. The analysis shows that FLC substantially reduces the peak acceleration fluctuations associated with the implemented SMC, with a maximum reduction of 97.5% in peak vertical acceleration relative to the SMC response.

In this paper, the mathematical model of full active suspension system is first reviewed in section 2, the proposed controllers are then introduced and discussed in section 3, then in section 4 numerical simulations of the proposed control schemes are presented and compared. Finally, the concluding remarks are given in section 5.

2. Mathematical Modeling of Full Active Suspension System

A comprehensive four-wheel dynamic model of a vehicle suspension system was recently developed, as presented in the work by the authors of [14]. The model employed in this study is a 7-DOF full-vehicle vertical-ride model, developed specifically to investigate suspension dynamics and ride comfort. It incorporates the vertical heave motion of the sprung vehicle body, body pitch and roll motions, and the vertical motions of the four unsprung masses. The model does not include lateral/yaw dynamics, longitudinal vehicle dynamics, steering dynamics, or detailed tire-road interaction associated with vehicle handling. Tire-road interaction is represented only in the vertical direction through the road-displacement inputs and tire stiffness within the suspension model. Therefore, the terms full-vehicle model and full-car model in this study refer to the complete four-corner vertical suspension model, rather than a comprehensive vehicle-dynamics model incorporating handling and longitudinal motion.

The adopted 7-DOF model provides a suitable platform for investigating how decentralized control actions at the four suspension corners interact through the coupled heave, pitch, and roll dynamics of the sprung body. The present study therefore uses this model to compare SMC and FLC under identical full-vehicle conditions rather than to claim novelty in the vehicle model itself.

An illustrative representation of how an active suspension system can be applied to a four-wheel vehicle configuration is provided in **Figure 1**, offering a clearer view of the system architecture and its potential control points. This figure helps bridge the theoretical model with a practical visual aid, setting the stage for future control development and experimental validation.

The road profile introduces varying vertical displacements at each of the vehicle's wheels, depending on the surface irregularities beneath them. These variations cause the vehicle body to respond not only with vertical motion (i.e., bounce), but also with changes in its pitching and rolling behavior. In other words, the mechanical dynamics of a complete vehicle suspension system can be described by the vertical motion of the sprung mass (i.e., the vehicle body), along with its pitching (i.e., tilting forward or backward) and rolling (i.e., tilting side to side), in response to road conditions. Additionally, the unsprung masses, which represent the wheel and suspension assemblies, also experience vertical bouncing at each corner of the vehicle. These collective motions together define the dynamic behavior of the full vehicle model, as captured in the study by Al-Jarrah *et al*. [14] as :

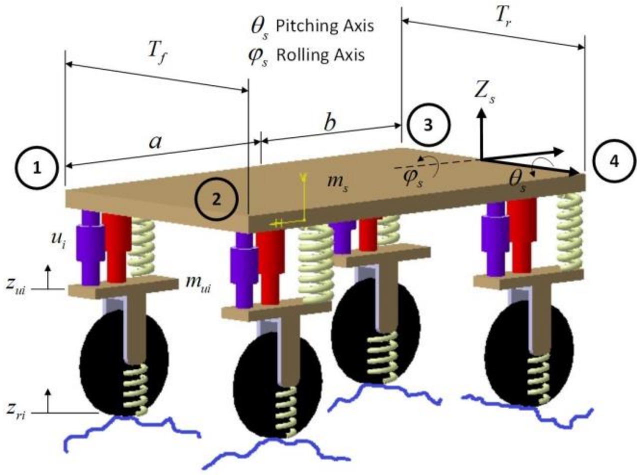

Figure 1. Active suspension system for a full vehicle model.

$$m_s\ddot{Z}_s = -b_f(\dot{z}_{s1} - \dot{z}_{u1}) - b_f(\dot{z}_{s2} - \dot{z}_{u2}) - b_r(\dot{z}_{s3} - \dot{z}_{u3}) - b_r(\dot{z}_{s4} - \dot{z}_{u4}) - k_f(z_{s1} - z_{u1}) - k_f(z_{s2} - z_{u2}) - k_r(z_{s3} - z_{u3}) - k_r(z_{s4} - z_{u4}) + u_1 + u_2 + u_3 + u_4 \tag{1}$$

$$I_P\ddot{\theta}_s = -b_f a(\dot{z}_{s1} - \dot{z}_{u1}) - b_f a(\dot{z}_{s2} - \dot{z}_{u2}) + b_r b(\dot{z}_{s3} - \dot{z}_{u3}) + b_r b(\dot{z}_{s4} - \dot{z}_{u4}) - k_f a(z_{s1} - z_{u1}) - k_f a(z_{s2} - z_{u2}) + k_r b(z_{s3} - z_{u3}) + k_r b(z_{s4} - z_{u4}) + au_1 + au_2 - bu_3 - bu_4 \tag{2}$$

$$I_r\ddot{\varphi}_s = -b_f T_f(\dot{z}_{s1} - \dot{z}_{u1}) + b_f T_f(\dot{z}_{s2} - \dot{z}_{u2}) - b_r T_r(\dot{z}_{s3} - \dot{z}_{u3}) + b_r T_r(\dot{z}_{s4} - \dot{z}_{u4}) - k_f T_f(z_{s1} - z_{u1}) + k_f T_f(z_{s2} - z_{u2}) - k_r T_r(z_{s3} - z_{u3}) + k_r T_r(z_{s4} - z_{u4}) + T_f u_1 - T_f u_2 + T_r u_3 - T_r u_4 \tag{3}$$

$$m_{ur}\ddot{z}_{u3} = b_f(\dot{z}_{s3} - \dot{z}_{u3}) + k_f(z_{s3} - z_{u3}) - k_{tf}z_{u3} + k_{tf}z_{r3} - u_3 \tag{4}$$

$$m_{uf}\ddot{z}_{u2} = b_f(\dot{z}_{s2} - \dot{z}_{u2}) + k_f(z_{s2} - z_{u2}) - k_{tf}z_{u2} + k_{tf}z_{r2} - u_2 \tag{5}$$

$$m_{ur}\ddot{z}_{u3} = b_f(\dot{z}_{s3} - \dot{z}_{u3}) + k_f(z_{s3} - z_{u3}) - k_{tf}z_{u3} + k_{tf}z_{r3} - u_3 \tag{6}$$

$$m_{ur}\ddot{z}_{u4} = b_f(\dot{z}_{s4} - \dot{z}_{u4}) + k_f(z_{s4} - z_{u4}) - k_{tf}z_{u4} + k_{tf}z_{r4} - u_4 \tag{7}$$

where

$$\dot{z}_{s1} = T_f\dot{\varphi}_s + a\dot{\theta}_s + \dot{Z}_s, z_{s1} = T_f\varphi_s + a\theta_s + Z_s \tag{8}$$

$$\dot{z}_{s2} = -T_f\dot{\varphi}_s + a\dot{\theta}_s + \dot{Z}_s, z_{s2} = -T_f\varphi_s + a\theta_s + Z_s \tag{9}$$

$$\dot{z}_{s3} = T_r\dot{\varphi}_s - b\dot{\theta}_s + \dot{Z}_s, z_{s3} = T_r\varphi_s - b\theta_s + Z_s \tag{10}$$

$$\dot{z}_{s4} = -T_r\dot{\varphi}_s - b\dot{\theta}_s + \dot{Z}_s, z_{s4} = -T_r\varphi_s - b\theta_s + Z_s \tag{11}$$

3. Proposed Controllers Formulation

The full-vehicle suspension constitutes a coupled MIMO plant because actuator actions at individual corners influence the common sprung-body heave, pitch, and roll dynamics. In this study, a decentralized control architecture is adopted in which each suspension actuator is governed by a local SISO controller. Two nonlinear control strategies, SMC and FLC, are implemented and compared under identical full-vehicle conditions. The local control laws do not explicitly require the complete 7-DOF vehicle model for online computation, while the coupling among the four suspension corners is retained through the full-vehicle dynamics.

The proposed controllers are designed to minimize the bouncing of the sprung vehicle body, as illustrated in **Figure 1**, to enhance ride comfort through the active suspension system. This requires the active suspension wheel actuator to generate precise control forces in order to effectively regulate the vertical acceleration and displacement of the sprung vehicle body to maintain optimal comfort levels.

3.1. Sliding Mode Controller

SMC is a nonlinear variable-structure control technique widely used because of its disturbance-rejection characteristics and robustness to certain classes of matched uncertainties (i.e., modeling errors and disturbances). Usually, a switching function is used to force the system to switch between two structures where both structures are primarily unstable. **Figure 2a** shows the phase portrait of a general system with one of the structures. This structure has an unstable equilibrium point focus at the origin, and from any starting point, the system plot in the phase diagram will spiral outwards to instability. On the other hand, **Figure 2b** shows the phase portrait of the same controlled system but with another structure where the phase plot shows a sudden equilibrium point at the origin.

As previously mentioned, both configurations illustrated in **Figure 2** are individually unstable. However, it is important to observe that in the second structure, a particular motion pattern can lead the system toward stability; specifically, along the line $s = \lambda e + \dot{e} = 0$ corresponding to the second configuration shown in **Figure 2b**. This insight forms the basis for applying a switching control strategy. By implementing a control law such as the one described in (12) and switching the system dynamics around the line s in Figure 2.b, the state trajectories of the two unstable structures begin to alternate in a coordinated way. This switching causes all trajectories to converge toward the sliding surface defined by s = 0, resulting in a stable sliding motion that guides the system smoothly toward the origin, as illustrated in **Figure 3**. This behavior highlights a fundamental

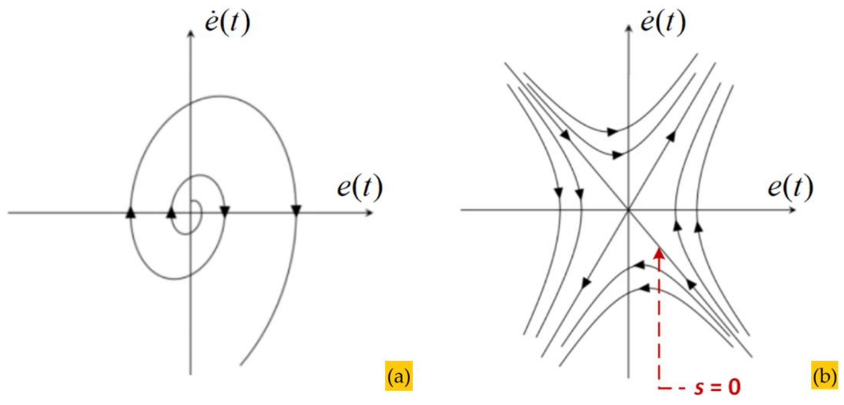

Figure 2. Dynamic responses and phase portraits of two unstable system structures

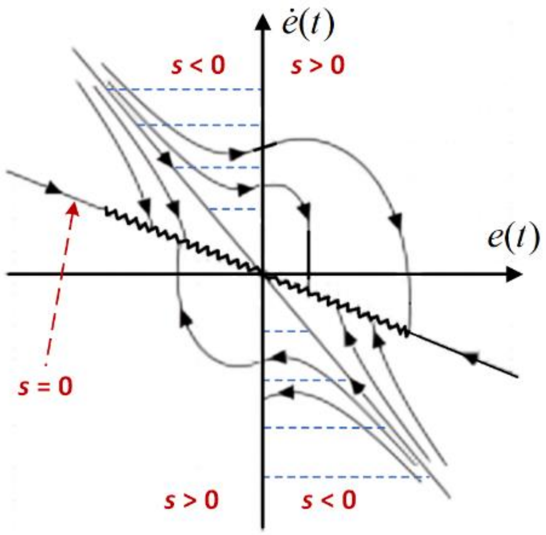

Figure 3. Asymptotically stable variable structure system consisting of the two unstable structures shown in Figure 2

principle of sliding mode control: stability is achieved not through the stability of individual structures, but through the intentional variation of the system's structure during the control process.

In general, two modes are recognized while using SMCs as shown in Figure 4: (i) the reaching mode and (ii) the sliding mode. The reaching mode is moving from point A until reaching the sliding surface (i.e., entering the sliding mode). In the sliding mode, the controller switches between two values based on the switching law until it reaches zero error. The SMC can be recognized in the form of a relay control law as:

$$u_i = ke_i \tag{12}$$

where

$$k = \begin{cases} \gamma_1, s > 0 \\ \gamma_2, s < 0 \end{cases} \tag{13}$$

$$s = \lambda e_i + \dot{e}_i \tag{14}$$

It is important to note that the error in the active suspension system is defined as the difference between the desired and the actual sprung mass vertical displacement at each wheel such that

$$e_i = z_{sdi} - z_{si} \tag{15}$$

where Z_{sdi} is set to ZERO. Note that each actuator in the active suspension is controlled by an individual SM controller.

As mentioned earlier, the controller switches between two values. This switching causes a chattering phenomenon which causes, in turn, a high frequency of the control device. This indeed affects its functionality over a short period of time (i.e., high controller activity cost). Hence, chattering is undesirable and should be eliminated or minimized for practical controller implementation. Other practical forms of SMC can be proposed instead as follows

$$u_i = k_1 e_i + k_2 \dot{e}_i \tag{16}$$

where

$$k_1 = \begin{cases} +\alpha_1, se_i > 0 \\ -\alpha_2, se_i < 0 \end{cases} \tag{17}$$

$$k_2 = \begin{cases} +\beta_1, s\dot{e}_i > 0 \\ -\beta_2, s\dot{e}_i < 0 \end{cases} \tag{18}$$

From the last three equations, it is evident that the switching functions are governed by the sign of the product involving the sliding surface, introduced in Eq. (14), the error signal, as shown in Eq. (17), and its time derivative, as shown in Eq. (18). This design provides a switching mechanism that selects the control action according to the signs of the sliding surface, error signal, and error first-time derivative. The resulting control law, as described in Eq. (16), ensures that the system switches appropriately between two inherently unstable structures. Through this coordinated switching, the system trajectories are driven toward and maintained on the sliding surface, ultimately achieving a stable response, as illustrated in Figure 3.

3.2. *Fuzzy Logic Controller*

FLC (i.e., rule-based, non-model-based control approach) is a soft computing technique that imitates the ability of the human mind to learn and make rational decisions. FLC has many advan-

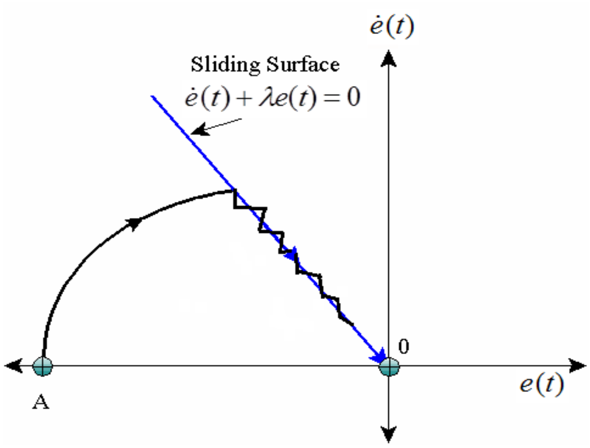

Figure 4. Phase plane portrait showing SMC

tages such as simplicity in implementation and a non-model-based approach. FLC is also effective in the cases of nonlinear and time-varying systems compared with other control methods. FLC usually consists of four parts: fuzzification, knowledge base, fuzzy inference, and defuzzification, as shown in Figure 5. The Fuzzification part converts the input exact quantities into fuzzified quantities and represents them with the corresponding fuzzy ruleset (i.e., If-Then statements). The role of defuzzification is to convert the control quantities obtained by the fuzzy inference into the actual quantities used for the control.

Figure 6 shows the suspension system block diagram where a FLC is designed and applied. Two inputs are used to develop the FLC: (i) the error signal, defined in (15), and (ii) its first-time derivative. The output of the proposed FLC is the active suspension wheel actuator force required to minimize the error at each corner of the vehicle, hence, reducing the roll and pitch angles and, as a result, securing a ride comfort.

Figure 7 and Figure 8 illustrate the structure of the proposed FLC, showcasing its input-output relationship and the resulting control surface derived from the fuzzy rule base. The complete set of fuzzy rules is provided in Table 1. For each input and output variable, seven membership functions have been defined, as shown in the table. These are expressed using common linguistic terms: Negative Large (NL), Negative (N), Negative Small (NS), Zero (Z), Positive Small (PS), Positive (P), and Positive Large (PL). Based on these terms, the controller assigns a degree of membership that helps determine the system's output in response to varying input conditions.

4. Numerical Testing and Verifications

This section presents numerical simulations conducted in MATLAB/Simulink environment to evaluate the effectiveness of the proposed controllers, as defined in (16) to (18) and illustrated in Figure 6, Figure 7, and Figure 8, in regulating the vertical motion, pitch, and roll of the full vehicle body. The simulations were executed using the ode8 (Dormand–Prince) solver with a fixed step size of 0.01 s. This step size was selected to provide sufficient temporal resolution for the investigated suspension dynamics while maintaining manageable computational cost.

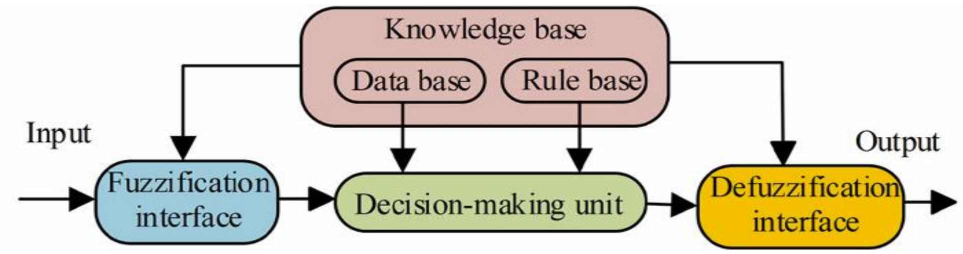

Figure 5. Structure and components of FL-based systems

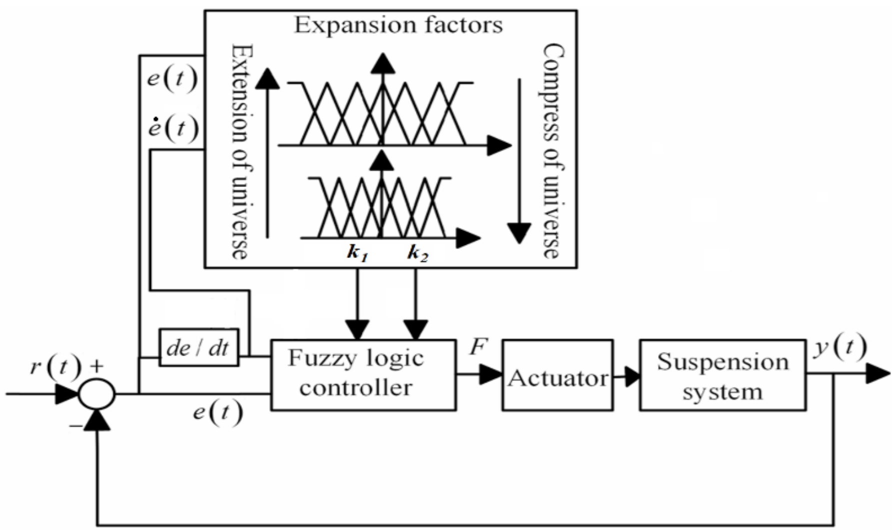

Figure 6. FLC block diagram for full vehicle active suspension system

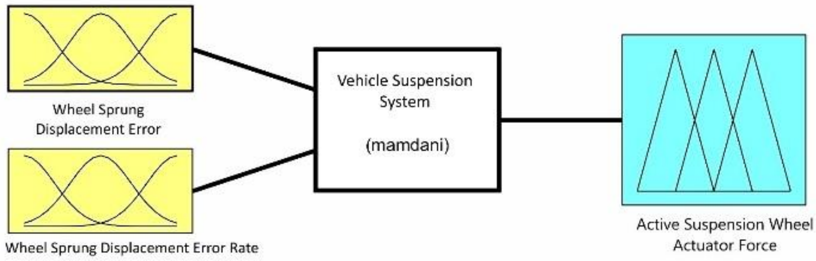

Figure 7. Layout of the FLC input and output structure

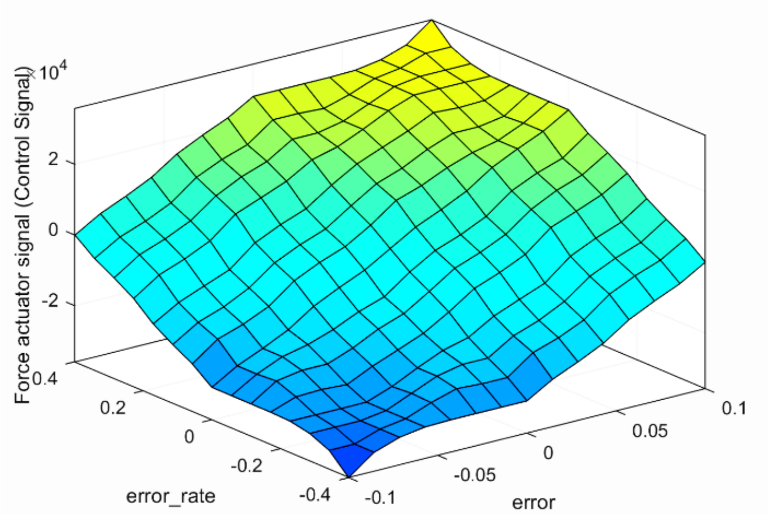

Figure 8. Control surface generated by the proposed FLC rule base

Table 1. Set of If-Then fuzzy rules used in the FL controller

If-Then Rules		$e(t)$				
		NL	N	Z	P	PL
$\dot{e}(t)$	NL	NL	N	N	NS	Z
	N	N	N	NS	Z	PS
	Z	N	NS	Z	PS	P
	P	NS	Z	PS	P	P
	PL	Z	PS	P	P	PL

4.1. *Settings of System Parameters and Testing*

The parameters of the full-vehicle suspension system used in the numerical study are provided in **Table 2**. Three deterministic road-disturbance profiles were selected to evaluate transient controller performance under severe asymmetric excitation. Unlike stochastic road profiles characterized using standards such as ISO 8608, the profiles considered here consist of discrete bumps, humps, and harmonic disturbances intended to produce repeatable transient excitation. Case 1 represents isolated severe vertical disturbances (**Figure 9**), whereas Cases 2 and 3 introduce phase differences among the four wheel inputs to deliberately excite coupled heave, pitch, and roll motions (**Figure 10** and **Figure 11**).

The maximum and minimum disturbance amplitudes of +20 cm and −15 cm were intentionally selected as severe stress-test inputs rather than as representations of normal highway roughness or specific ISO 8608 road classes. These amplitudes represent localized extreme obstacles, such as severe bumps or pothole-like disturbances, and are used to examine controller behavior under high-amplitude transient excitation. Accordingly, the selected profiles should be interpreted as deterministic worst-case numerical benchmarks for comparative controller evaluation rather than standardized road-roughness profiles.

In addition, two performance measures were utilized to evaluate how good the proposed controllers are and to quantify the quality of performance. The performance measures are ERM and puEFM and are expressed as

$$ERM \triangleq \int_0^T \sqrt{(Z_{sd}-Z_s)^2+(\theta_{sd}-\theta_s)^2+(\varphi_{sd}-\varphi_s)^2} \quad (19)$$

$$puEFM \triangleq \left(\frac{\int_0^T \sqrt{(u_1)^2+(u_2)^2+(u_3)^2+(u_4)^2}}{EFM|_{max}}\right) \quad (20)$$

where ERM is the error measure, puEFM is the per unit effort measure, and $EFM|_{max}$ is the maximum EFM, and T is the entire simulation time.

Table 2. Full vehicle suspension system parameter values

Parameter	Value	Parameter	Value
a	1.4	m_s	1500
b	1.7	m_{uf}	59
I_p	2160	m_{ur}	59
I_r	460	T_f	0.505
k_{tf}	19000	T_r	0.507
k_{tr}	19000	-	-

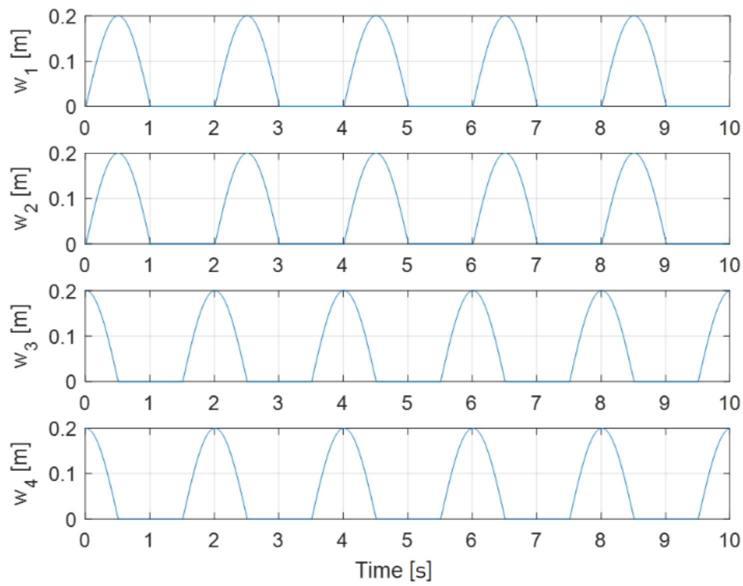

Figure 9. Simulated disturbance for Case 1 for all wheels (i.e., vehicle corners)

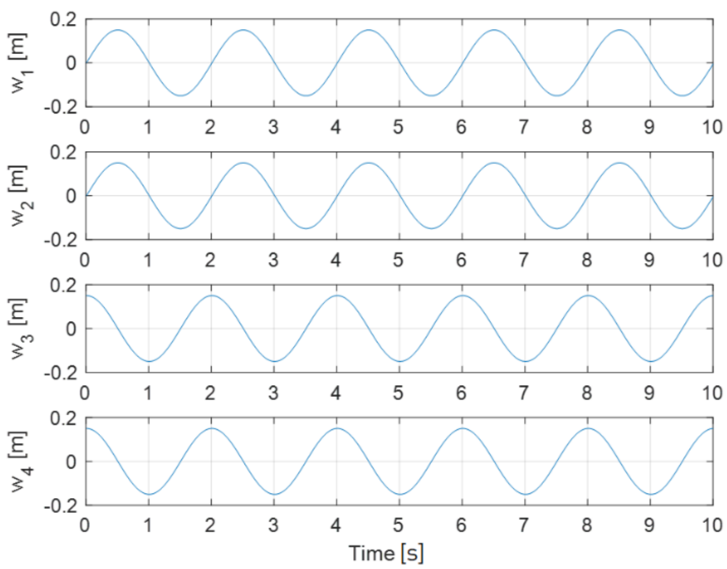

Figure 10. Simulated disturbance for Case 2 for all wheels (i.e., vehicle corners)

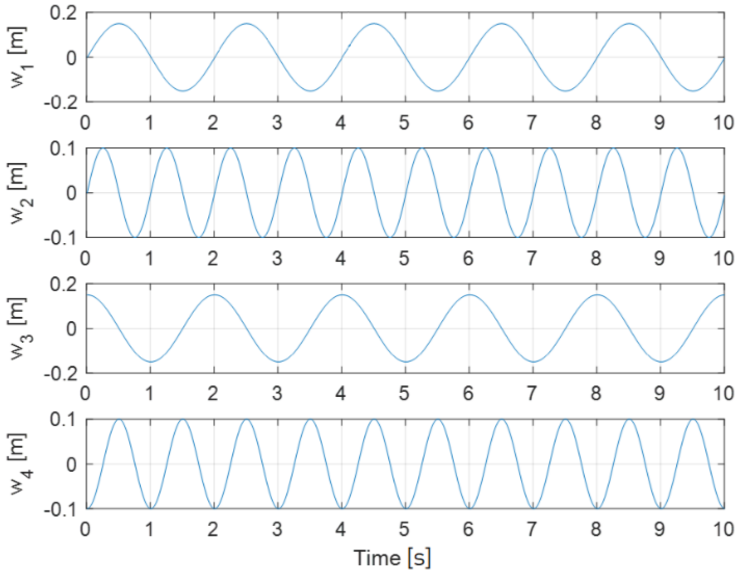

Figure 11. Simulated disturbance for Case 3 for all wheels (i.e., vehicle corners)

4.2. *Numerical Simulations*

The behavior of the selected full vehicle active suspension system (refer to **Table 2**) is demonstrated in **Figure 12** to **Figure 23** for all cases, which are introduced and demonstrated in **Figure 3**. The simulation results presented in **Figure 12** to **Figure 23** highlight the effectiveness of the proposed SMC and FLC in mitigating the vertical, pitch, and roll motions of a full vehicle model subjected to challenging road disturbances. Both controllers significantly outperform the passive suspension system in terms of displacement and overall stability, validating the need for active suspension systems in improving ride comfort (**Figure 12**, **Figure 13**, **Figure 14**, and **Figure 21**). To further challenge the proposed controllers, some simulation cases were designed to introduce time-varying parameters, such as a changing spring constant (e.g., Case 3) and stiffness variations (e.g., Cases 2 and 3), which can represent aging effects in suspension components (**Figure 15**, **Figure 16**, **Figure 17**, **Figure 18Figure 19**, **Figure 19**, **Figure 20**, **Figure 22**, and **Figure 23**).

Notably, FLC provides lower vertical acceleration than the implemented SMC across the investigated disturbance cases. This behavior is primarily associated with the continuous rule-based control action of FLC, whereas the switching action of the implemented SMC generates larger high-frequency acceleration fluctuations. The results therefore indicate an advantage of FLC in vibration suppression within the specific vehicle model and disturbance scenarios considered in this study.

Table 3. Disturbance cases introduced to investigate the performance of the proposed SM and FL controllers

Case	Disturbance Mathematical Expression
1	$w_1 = w_2 = 0.2\,sin(\pi t)\left(\frac{sgn(sin(\pi t)) + 1}{2}\right)$ $w_3 = w_4 = 0.2\,sin(\pi t - 3.5\pi)\left(\frac{sgn(sin(\pi t - 3.5\pi)) + 1}{2}\right)$ $b_f = b_r = 600,\ k_f = 35000,\ k_r = 38000$
2	$w_1 = w_2 = 0.15\,sin(\pi t), \quad w_3 = w_4 = 0.15\,sin(\pi t - 3.5\pi)$ $b_f = 0.2 \times 600\,sin(2\pi) + 600,\ b_r = 0.3 \times 600\,sin\left(\frac{\pi}{2}\right) + 600,\ k_f = 35000,\ k_r = 38000$
3	$w_1 = 0.15\,sin(\pi t), \quad w_2 = 0.1\,sin(2\pi t)$ $w_3 = 0.15\,sin(\pi t - 3.5\pi), \quad w_4 = 0.1\,sin(2\pi t - 2.5\pi)$ $b_f = 0.2 \times 600\,sin(2\pi) + 600,\ b_r = 0.3 \times 600\,sin\left(\frac{\pi}{2}\right) + 600,$ $k_f = 0.15 \times 35000\,sin(2\pi) + 35000,\ k_r = 0.15 \times 38000\,sin\left(\frac{\pi}{2}\right) + 38000$

In contrast, while the SMC effectively reduces displacement and maintains system stability, it exhibits chattering behavior—an inherent issue in classical SMC design. This high-frequency switching not only increases control effort but may also lead to premature actuator wear in practical applications. Although the SMC shows good disturbance-rejection performance characteristics, its aggressive control strategy results in higher acceleration fluctuations compared to the FLC, potentially compromising ride comfort.

The quantified performance metrics, particularly ERM and puEFM, reinforce these observations. As shown in Table 4, the FLC achieves significantly lower ERM values across all disturbance cases, indicating better tracking accuracy and smoother responses. While both controllers require comparable normalized control effort, the smoother response obtained with FLC suggests potential advantages for future real-time implementation, particularly with respect to passenger vibration exposure and actuator

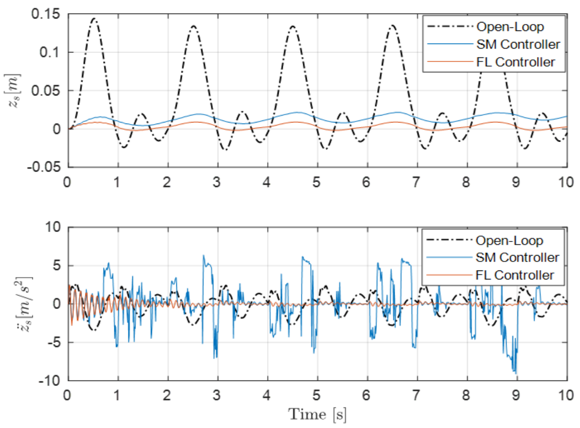

Figure 12. Simulated sprung vehicle body vertical displacement and acceleration for Case 1

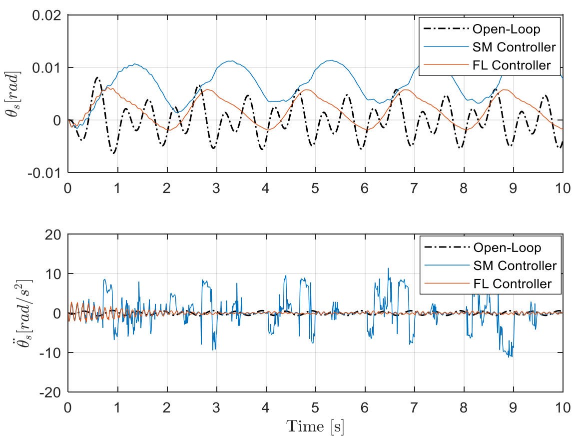

Figure 13. Simulated sprung vehicle body pitching angle and acceleration for Case 1

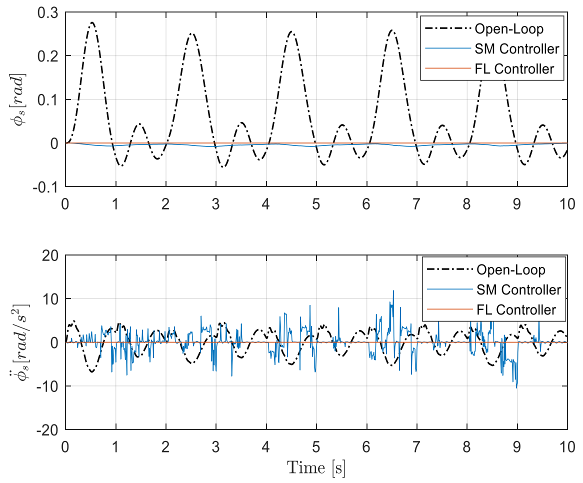

Figure 14. Simulated sprung vehicle body rolling angle and acceleration for Case 1

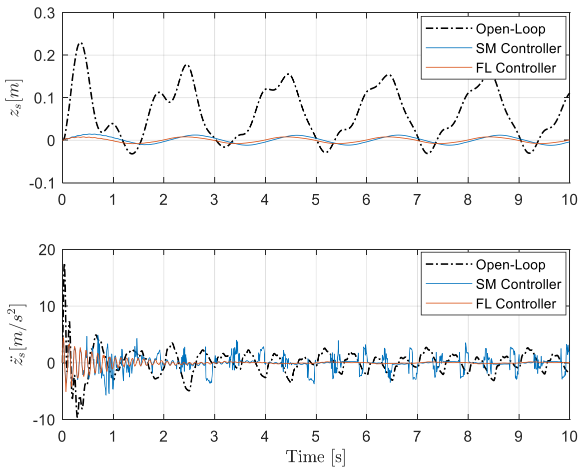

Figure 15. Simulated sprung vehicle body vertical displacement and acceleration for Case 2

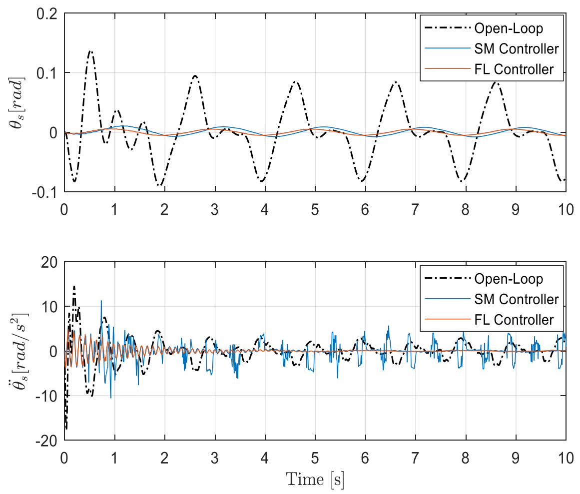

Figure 16. Simulated sprung vehicle body pitching angle and acceleration for Case 2

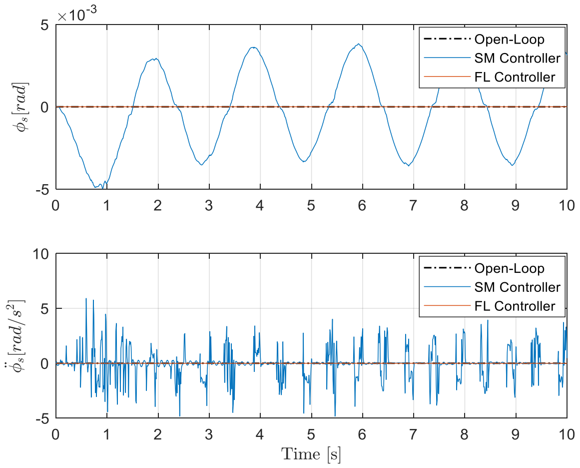

Figure 17. Simulated sprung vehicle body rolling angle and acceleration for Case 2

ctivity. However, this potential must be confirmed through HIL and experimental testing.

The reduction percentages in **Table 5** further demonstrate the superior performance of FLC relative to SMC, achieving up to a 97.5% reduction in peak vertical acceleration and approximately 69.5% in maximum vertical displacement. These results highlight the smoother vibration-suppression characteristics of FLC compared with the implemented SMC, particularly in reducing acceleration fluctuations associated with SMC switching behavior. Note that the reduction percentages for the vertical displacement and acceleration are calculated as:

$$\mathrm{RP_d} \triangleq \left(1 - \frac{\mathrm{Z_{s-max-FLC}}}{\mathrm{Z_{s-max-SMC}}}\right) \times 100\% \tag{20}$$

$$\mathrm{RP_a} \triangleq \left(1 - \frac{\ddot{\mathrm{Z}}_{\mathrm{s-max-FLC}}}{\ddot{\mathrm{Z}}_{\mathrm{s-max-SMC}}}\right) \times 100\% \tag{21}$$

where $Z_{s-max-SMC}$ and $Z_{s-max-FLC}$ are the maximum Z_s when using SMC and FLC, respectively, and $\ddot{Z}_{s-max-SMC}$ and $\ddot{Z}_{s-max-FLC}$ are the maximum $\ddot{Z}_s$ when using SMC and FLC, respectively.

It should be emphasized that the reduction percentages reported in **Table 5** are calculated using SMC as the comparative reference. In particular, the maximum reduction of 97.5% refers to the peak vertical acceleration obtained with FLC relative to the corresponding peak value produced by the implemented SMC. This unusually large percentage primarily reflects the sensitivity of the peak-acceleration metric to the switching-induced acceleration spikes associated

Table 4. Performance measures for the proposed SMC in comparison with the FLC for the disturbance cases described in Table 3 where $|e_s|_{mss}$ is the maximum steady-state absolute tracking error and $e_s \triangleq Z_{sd} - Z_s$ where Z_{sd} is set to ZERO

Case	SMC			FLC		
	$\lvert e_s\rvert_{mss}$	ERM	puEFM	$\lvert e_s\rvert_{mss}$	ERM	puEFM
1	0.0214	0.1633	0.8839	0.0089	0.0498	0.6389
2	0.0119	0.1010	1	0.0079	0.0655	0.8860
3	0.0077	0.0996	0.7832	0.0061	0.0704	0.7084

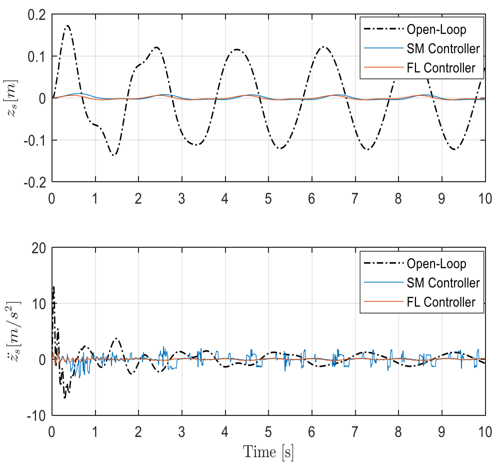

Figure 18. Simulated sprung vehicle body vertical displacement and acceleration for Case 3

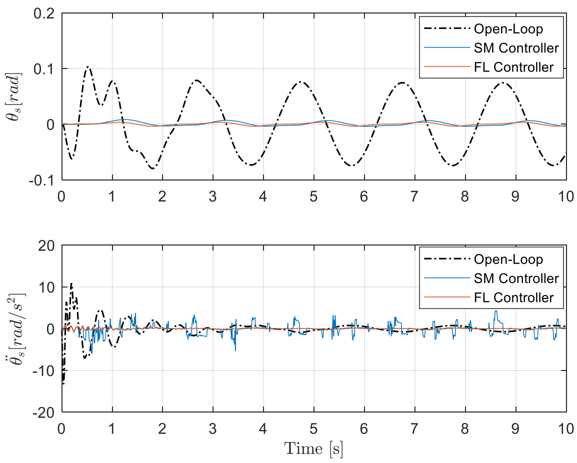

Figure 19. Simulated sprung vehicle body pitching angle and acceleration for Case 3

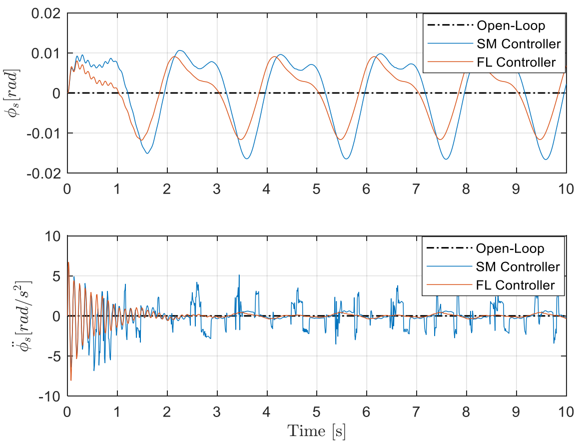

Figure 20. Simulated sprung vehicle body rolling angle and acceleration for Case 3

with the classical SMC implementation. The continuous fuzzy inference mechanism produces a considerably smoother control action and therefore avoids these large instantaneous peaks.

Accordingly, the 97.5% value should be interpreted specifically as a reduction in the maximum acceleration peak under the investigated conditions, rather than as a 97.5% improvement in all ride-comfort measures. A formal passenger-comfort classification would additionally require frequency-weighted acceleration evaluation according to standards such as ISO 2631-1.

Table 5. Reduction percentages in maximum vertical displacement and peak vertical acceleration achieved by FLC relative to SMC

Case	RP_d	RP_a
1	69.5	97.5
2	35.15	96.67
3	29.32	91.76

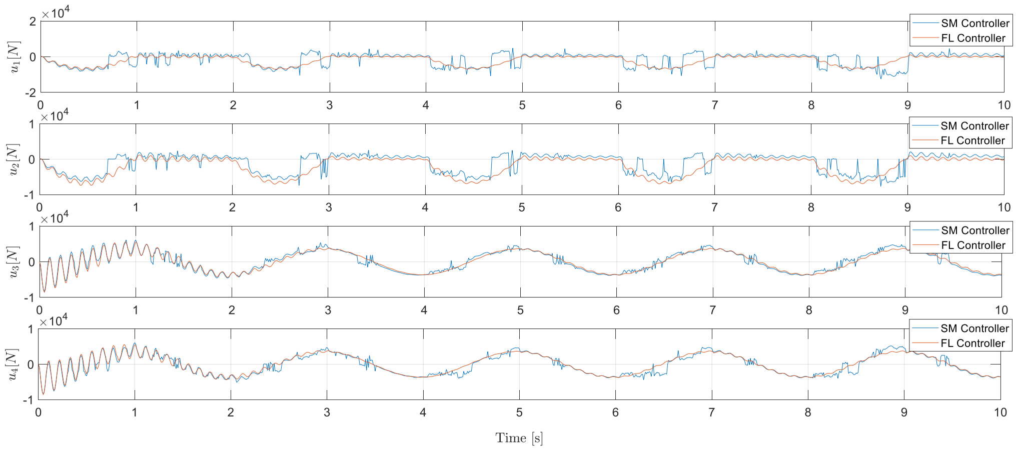

Figure 21. Simulated full active suspension actuators' forces on all wheels (i.e., vehicle corners) for Case 1

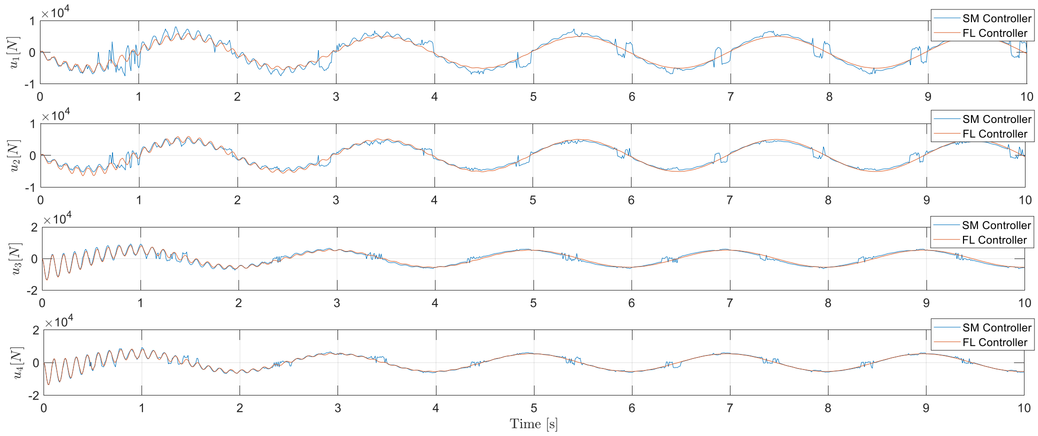

Figure 22. Simulated full active suspension actuators' forces on all wheels (i.e., vehicle corners) for Case 2

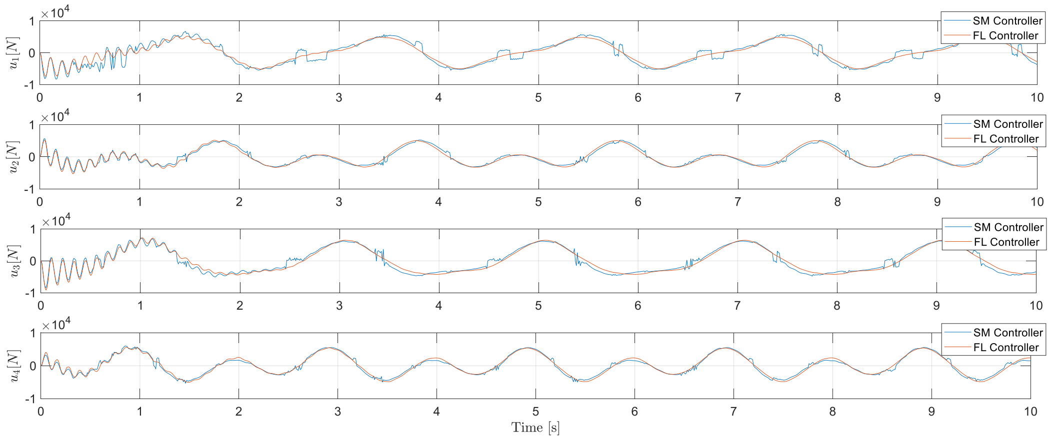

Figure 23. Simulated full active suspension actuators' forces on all wheels (i.e., vehicle corners) for Case 3

5. Conclusion

This study comparatively evaluated decentralized SMC and FLC strategies for a 7-DOF full-vehicle active suspension system under three severe asymmetric road-disturbance scenarios. The four local controllers operate on a coupled vehicle plant and collectively regulate sprung-body heave, pitch, and roll motions. Under the investigated conditions, both active controllers effectively suppressed vehicle-body vibration, while FLC provided superior acceleration attenuation relative to the implemented SMC. Specifically, FLC reduced the maximum vertical displacement by up to 69.5% and the peak vertical acceleration by up to 97.5% relative to SMC, while maintaining a maximum steady-state tracking error below 0.89 cm and comparable normalized control effort.

The particularly large reduction in peak acceleration is primarily associated with the smoother control action of FLC and the suppression of the switching-induced acceleration peaks observed with the implemented classical SMC. Therefore, this percentage represents improvement in the peak-acceleration metric under the investigated simulation conditions and should not be interpreted as an equivalent percentage improvement in all ride-comfort measures.

The findings are limited to numerical simulations of the selected vertical-ride vehicle model and disturbance scenarios. Detailed actuator dynamics, hardware saturation, sensor noise, real-time processor limitations, and comprehensive road-holding and handling metrics were not investigated. Future work will therefore focus on hardware-in-the-loop testing, full-scale experimental validation, formal ISO 2631-1 ride-comfort assessment, and evaluation across different vehicle parameters and operating conditions. Such investigations are necessary before broader conclusions regarding real-world controller performance can be established.

Author's Declaration

Authors' contributions and responsibilities

The authors made substantial contributions to the conception and design of the study. The authors took responsibility for data analysis, interpretation and discussion of results. The authors read and approved the final manuscript.

Funding

This research received no external funding.

Availability of data and materials

All data are available from the authors.

Competing interests

The authors declare no competing interest.

Generative AI statement

During the preparation of this manuscript, the authors used ChatGPT (OpenAI) solely to improve the language, grammar, and readability of a limited number of passages. The tool was not used to generate scientific content, conduct analyses, interpret results, or draw conclusions. All AI-assisted revisions were carefully reviewed and, where necessary, edited by the authors, who take full responsibility for the final content of the manuscript.

Additional information

No additional information from the authors.

References

[1] I.-H. Li and L.-W. Lee, "Design and Development of an Active Suspension System Using Pneumatic-Muscle Actuator

and Intelligent Control," *Applied Sciences*, vol. 9, no. 20, p. 4453, Oct. 2019, doi: 10.3390/app9204453.

[2] S.-Y. Han and T. Liang, "Reinforcement-Learning-Based Vibration Control for a Vehicle Semi-Active Suspension System via the PPO Approach," *Applied Sciences*, vol. 12, no. 6, p. 3078, Mar. 2022, doi: 10.3390/app12063078.

[3] M. Salah, "A laboratory automotive suspension test rig: design, implementation, and integration," *Jordan Journal of Mechanical and Industrial Engineering*, vol. 11, no. 2, pp. 67–71, 2017.

[4] C. M. Ho, D. T. Tran, and K. K. Ahn, "Adaptive sliding mode control based nonlinear disturbance observer for active suspension with pneumatic spring," *Journal of Sound and Vibration*, vol. 509, p. 116241, Sep. 2021, doi: 10.1016/j.jsv.2021.116241.

[5] K. Bayar and F.-S. Khaneghah, "Optimal Sliding Mode Control Method for Active Suspension Control," *IFAC-PapersOnLine*, vol. 53, no. 2, pp. 14285–14291, 2020, doi: 10.1016/j.ifacol.2020.12.1178.

[6] D. Quaini, K. Sazgetdinov, V. Ivanov, and A. Ferrara, "Optimization Based Sliding Mode Control in Active Suspensions: Design and Hardware-in-the-Loop Assessment," in *2020 European Control Conference (ECC)*, St. Petersburg, Russia: IEEE, May 2020, pp. 1607–1612. doi: 10.23919/ECC51009.2020.9143835.

[7] R. Bai and D. Guo, "Sliding-Mode Control of the Active Suspension System with the Dynamics of a Hydraulic Actuator," *Complexity*, vol. 2018, no. 1, p. 5907208, Jan. 2018, doi: 10.1155/2018/5907208.

[8] Y. Md. Sam, J. H. S. Osman, and M. R. Abd. Ghani, "Sliding Mode Control of Active Suspension System," *Jurnal Teknologi*, vol. 37, pp. 370–375, Jan. 2012, doi: 10.11113/jt.v37.534.

[9] D. N. Nguyen, T. A. Nguyen, and N. D. Dang, "A Novel Sliding Mode Control Algorithm for an Active Suspension System Considering with the Hydraulic Actuator," *Latin American Journal of Solids and Structures*, vol. 19, no. 1, 2022, doi: 10.1590/1679-78256883.

[10] M. A. M. Obaid, A. R. Husain, and A. A. Mohammed Al-kubati, "Intelligent Sliding Mode Controller for Active Suspension System Using Particle Swarm Optimization," *Jurnal Teknologi*, vol. 69, no. 1, Jun. 2014, doi: 10.11113/jt.v69.2168.

[11] Hung-Yi Chen and Shiuh-Jer Huang, "Adaptive Sliding Controller for Active Suspension System," in *2005 International Conference on Control and Automation*, Budapest: IEEE, Mar. 2011, pp. 282–287. doi: 10.1109/ICCA.2005.1528132.

[12] H. Chen and K. Guo, "Constrained H∞ control of active suspension systems with time-varying input delay," *IEEE Transactions on Control Systems Technology*, vol. 13, no. 5, pp. 791–798, 2005, doi: 10.1243/09544070JAUTO299.

[13] A. Alleyne and J. K. Hedrick, "Nonlinear adaptive control of active suspensions," *IEEE Transactions on Control Systems Technology*, vol. 3, no. 1, pp. 94–101, Mar. 1995, doi: 10.1109/87.370714.

[14] A. Al-Jarrah, A. Al-Tamimi, S. Banihani, and M. Salah, "State Feedback-Based H2 Optimal Control for a Full Vehicle Active Suspension System," *International Review of Automatic Control (IREACO)*, vol. 17, no. 3, p. 84, May 2024, doi: 10.15866/ireaco.v17i3.24882.

[15] L. Wu, W. Zhang, L. Ni, W. Jia, and I. Youn, "Attitude Tracking Control of All-Terrain Vehicle with Tandem Active–Passive Suspension," *International Journal of Automotive Technology*, vol. 25, no. 5, pp. 1091–1111, Oct. 2024, doi: 10.1007/s12239-024-00085-9.

[16] J.-S. Lin and C.-J. Huang, "Nonlinear Backstepping Active Suspension Design Applied to a Half-Car Model," *Vehicle System Dynamics*, vol. 42, no. 6, pp. 373–393, Dec. 2004, doi: 10.1080/004231104200266784.

[17] C. Gohrle, A. Schindler, A. Wagner, and O. Sawodny, "Design and Vehicle Implementation of Preview Active Suspension Controllers," *IEEE Transactions on Control Systems Technology*, vol. 22, no. 3, pp. 1135–1142, May 2014, doi: 10.1109/TCST.2013.2272342.

[18] M. Salah, M. Ali, and S. Nabhan, "Robust Nonlinear Control for Automotive Active

Suspension Systems," in *2022 Australian & New Zealand Control Conference (ANZCC)*, Gold Coast, Australia: IEEE, Nov. 2022, pp. 29–33. doi: 10.1109/ANZCC56036.2022.9966973.

[19] C. Edwards and S. Spurgeon, *Sliding Mode Control*. CRC Press, 1998. doi: 10.1201/9781498701822.

[20] V. I. Utkin, *Sliding modes in control and optimization*. Springer-Verlag, 1992.

[21] H. Chen, P.-Y. Sun, and K.-H. Guo, "A multi-objective control design for active suspensions with hard constraints," in *Proceedings of the 2003 American Control Conference, 2003.*, IEEE, 2003, pp. 4371–4376. doi: 10.1109/ACC.2003.1240526.

[22] L. Ming, L. Yibin, R. Xuewen, Z. Shuaishuai, and Y. Yanfang, "Semi-Active Suspension Control Based on Deep Reinforcement Learning," *IEEE Access*, vol. 8, pp. 9978–9986, 2020, doi: 10.1109/ACCESS.2020.2964116.

[23] A. Al-Tamimi, S. Banihani, A. Al-Jarrah, and M. Salah, "Least Squares-Based Neural Network Controller for Stabilization of Full Vehicle Active Suspension Systems," *International Review of Automatic Control (IREACO)*, vol. 18, no. 2, p. 112, Mar. 2025, doi: 10.15866/ireaco.v18i2.25976.

[24] P. I. Ro, C. Kim, and H. Kim, "An Active Suspension System using Fuzzy Logic Control," in *1993 American Control Conference*, IEEE, Jun. 1993, pp. 2252–2253. doi: 10.23919/ACC.1993.4793285.

[25] A. S. Cherry and R. P. Jones, "Fuzzy logic control of an automotive suspension system," *IEE Proceedings - Control Theory and Applications*, vol. 142, no. 2, pp. 149–160, Mar. 1995, doi: 10.1049/ip-cta:19951736.

[26] J. L. Yester and R. H. McFall, "Fuzzy logic controller for active suspension," in *Proceedings of the Society of Automotive Engineers*, 1992, pp. 259–270.

[27] S. J. Huang and H. C. Chao, "Fuzzy logic controller for a vehicle active suspension system," *Proceedings of the Institution of Mechanical Engineers, Part I: Journal of Automobile Engineering*, vol. 214, pp. 1–12, 2000, doi: 10.1109/91.705510.

[28] Ji-Chang Lo and Ya-Hui Kuo, "Decoupled fuzzy sliding-mode control," *IEEE Transactions on Fuzzy Systems*, vol. 6, no. 3, pp. 426–435, 1998, doi: 10.1109/91.705510.

[29] Chun-Yi Su and Y. Stepanenko, "Adaptive control of a class of nonlinear systems with fuzzy logic," *IEEE Transactions on Fuzzy Systems*, vol. 2, no. 4, pp. 285–294, 1994, doi: 10.1109/91.324808.

[30] L.-X. Wang, "Stable adaptive fuzzy control of nonlinear systems," *IEEE Transactions on Fuzzy Systems*, vol. 1, no. 2, pp. 146–155, May 1993, doi: 10.1109/91.227383.

[31] W. Sun, H. Gao, and O. Kaynak, "Adaptive Backstepping Control for Active Suspension Systems With Hard Constraints," *IEEE/ASME Transactions on Mechatronics*, vol. 18, no. 3, pp. 1072–1079, Jun. 2013, doi: 10.1109/TMECH.2012.2204765.

[32] Y.-J. Liu and H. Chen, "Adaptive Sliding Mode Control for Uncertain Active Suspension Systems With Prescribed Performance," *IEEE Transactions on Systems, Man, and Cybernetics: Systems*, vol. 51, no. 10, pp. 6414–6422, Oct. 2021, doi: 10.1109/TSMC.2019.2961927.

[33] W. Gang, "ESO-Based Terminal Sliding Mode Control for Uncertain Full-Car Active Suspension Systems," *International Journal of Automotive Technology*, vol. 21, no. 3, pp. 691–702, Jun. 2020, doi: 10.1007/s12239-020-0067-y.

[34] A. Levant, "Higher-order sliding modes, differentiation and output-feedback control," *International Journal of Control*, vol. 76, no. 9–10, pp. 924–941, Jan. 2003, doi: 10.1080/0020717031000099029.

[35] A. Levant and L. Fridman, "Higher-Order Sliding Modes," in *Sliding mode control in engineering*, CRC Press, 2002, pp. 53–102. doi: 10.1201/9780203910856.ch3.

[36] Y. Shtessel, C. Edwards, L. Fridman, and A. Levant, *Sliding mode control and observation*. Springer, 2014.

[37] G. Bartolini, L. Fridman, A. Pisano, and E. Usai, *Modern Sliding Mode Control Theory*, vol. 375. in Lecture Notes in Control and Information Sciences, vol. 375. Berlin, Heidelberg: Springer Berlin Heidelberg, 2008. doi: 10.1007/978-3-540-79016-7.

[38] Y. M. Sam, J. H. S. Osman, and M. R. A. Ghani, "A class of proportional-integral sliding mode control with application to active suspension system," *Systems & Control Letters*, vol. 51, no. 3–4, pp. 217–223, Mar. 2004, doi: 10.1016/j.sysconle.2003.08.007.

[39] S.-B. Choi and Y.-M. Han, "Vibration control of electrorheological seat suspension with human-body model using sliding mode control," *Journal of Sound and Vibration*, vol. 303, no. 1–2, pp. 391–404, Jun. 2007, doi: 10.1016/j.jsv.2007.01.027.